

Performance enhancement of IGZO thin-film transistors via ultra-thin HfO_2 and the implementation of logic device functionality

Xuyang Li(栗旭阳), Bin Liu(刘斌), Xianwen Liu(刘贤文), Shuo Zhang(张硕), Congyang Wen(温丛阳), Jin Zhang(张进), Haifeng Liang(梁海锋), Guangcai Yuan(袁广才), Jianshe Xue(薛建设), and Zhinong Yu(喻志农)

Citation: Chin. Phys. B, 2025, 34 (**7**): 076101. DOI: 10.1088/1674-1056/adcb22
http://cpb.iphy.ac.cn; http://iopscience.iop.org/cpb

What follows is a list of articles you may be interested in

Strategy to mitigate single event upset in 14-nm CMOS bulk FinFET technology

Dong-Qing Li(李东青), Tian-Qi Liu(刘天奇), Pei-Xiong Zhao(赵培雄), Zhen-Yu Wu(吴振宇), Tie-Shan Wang(王铁山), and Jie Liu(刘杰)

Chin. Phys. B, 2022, 31 (**5**): 056106. DOI: 10.1088/1674-1056/ac3d7e

Characterization, spectroscopic investigation of defects by positron annihilation, and possible application of synthesized PbO nanoparticles

Sk Irsad Ali, Anjan Das, Apoorva Agrawal, Shubharaj Mukherjee, Maudud Ahmed, P M G Nambissan, Samiran Mandal, and Atis Chandra Mandal

Chin. Phys. B, 2021, 30 (**2**): 026103. DOI: 10.1088/1674-1056/abd2a9

First-principles study of oxygen adsorbed on Au-doped RuO_2 (110) surface

Ji Zhang(张季), De-Ming Zhang(张德明)

Chin. Phys. B, 2019, 28 (**11**): 116107. DOI: 10.1088/1674-1056/ab4cdc

Mechanism of floating body effect mitigation via cutting off source injection in a fully-depleted silicon-on-insulator technology

Pengcheng Huang(黄鹏程), Shuming Chen(陈书明), Jianjun Chen(陈建军)

Chin. Phys. B, 2016, 25 (**3**): 036103. DOI: 10.1088/1674-1056/25/3/036103

Effects of annealing process on characteristics of fully transparent zinc tin oxide thin-film transistor

Chen Yong-Yue (陈勇跃), Wang Xiong (王雄), Cai Xi-Kun (才玺坤), Yuan Zi-Jian (原子健), Zhu Xia-Ming (朱夏明), Qiu Dong-Jiang (邱东江), Wu Hui-Zhen (吴惠桢)

Chin. Phys. B, 2014, 23 (**2**): 026101. DOI: 10.1088/1674-1056/23/2/026101

Performance enhancement of IGZO thin-film transistors via ultra-thin HfO_2 and the implementation of logic device functionality

Xuyang Li(栗旭阳)[1,†], Bin Liu(刘斌)[2], Xianwen Liu(刘贤文)[2], Shuo Zhang(张硕)[2], Congyang Wen(温丛阳)[2], Jin Zhang(张进)[1], Haifeng Liang(梁海锋)[1], Guangcai Yuan(袁广才)[3], Jianshe Xue(薛建设)[3], and Zhinong Yu(喻志农)[2,‡]

[1] *School of Optoelectronic Engineering, Xi'an Technological University, Xi'an* 710021, *China*
[2] *School of Optics and Photonics, Beijing Institute of Technology, Beijing* 100081, *China*
[3] *Beijing BOE Display Technology Co., Ltd., Beijing* 100176, *China*

(Received 28 February 2025; revised manuscript received 25 March 2025; accepted manuscript online 10 April 2025)

The enhancement of mobility has always been a research focus in the field of thin-film transistors (TFTs). In this paper, we report a method using ultra-thin HfO_2 to improve the electrical performance of indium gallium zinc oxide (IGZO) TFTs. HfO_2 not only repairs the surface morphology of the active layer, but also increases the carrier concentration. When the thickness of the HfO_2 film was 3 nm, the mobility of the device was doubled ($14.9\ cm^2\cdot V^{-1}\cdot s^{-1} \rightarrow 29.6\ cm^2\cdot V^{-1}\cdot s^{-1}$), and the device exhibited excellent logic device performance. This paper provides a simple and effective method to enhance the electrical performance of IGZO TFTs, offering new ideas and experimental foundation for research into high-performance metal oxide (MO) TFTs.

Keywords: thin-film transistors, metal oxide, indium gallium zinc oxide (IGZO), logic devices, TCAD simulation

PACS: 61.43.Dq, 61.82.Fk

DOI: 10.1088/1674-1056/adcb22 **CSTR:** 32038.14.CPB.adcb22

1. Introduction

Metal oxide (MO) thin-film transistors (TFTs) are widely used in display devices due to their high visible-light transmittance, good stability and excellent electrical performance.[1–3] Since they were first proposed as the mainstream MO TFTs, indium gallium zinc oxide (IGZO) TFTs have attracted extensive attention.[4–9] Characterized by advantages, such as low off-current, high mobility and wide band gap, IGZO TFTs have been extensively applied in display drivers, electronic skins and detectors.[10–13]

With the rapid development of the display industry, the demand for high-refresh-rate and high-definition displays has driven continuous improvement in the mobility of MO TFTs.[14,15] Enhancing the electrical performance of devices has always been a research focus in the field of MO TFTs. For example, using a dual-active-layer structure can boost MO TFT mobility. Two different active-layer materials will increase the carrier concentration and form a two-dimensional electron gas at the heterojunction interface, thus improving the electrical performance and stability of the devices.[16–20] However, requiring two types of semiconductor materials, this method raises device manufacturing costs. Some studies have treated the active layer with plasma to adjust the surface morphology of the thin film and the oxygen vacancy concentration in the active layer, thus enhancing the device electrical performance.[21–25] However, this method requires precise control of the plasma gas process, increasing the complexity of device manufacturing. Some studies have improved the stability of devices by controlling the annealing atmosphere (such as introducing argon or hydrogen during annealing).[26,27] However, the improvement effect of this method is limited. Recently, some studies on metal oxide capping layers modifying the active layer have gained attention, such as using alumina, calcium oxide, etc, as metal oxide capping layers to modify the active layer.[28–30] Typically, the metal oxide modification layer is placed above the active layer. This method not only prevents the active layer from contacting environmental water vapor, enhancing device environmental stability, but also increases carrier concentration within the active layer, significantly improving device electrical performance.

In this paper, we report on the impact of an ultra-thin hafnium dioxide (HfO_2) modification layer on the performance of IGZO TFTs. We deposited HfO_2 thin films of different thicknesses on the active layer of TFTs as a modification layer. We then analyzed the effect of the thickness of the modification layer on the performance of TFTs. The experimental results show that while HfO_2 can enhance device performance, an excessively thick modification layer is detrimental. We explained this experimental phenomenon by a combination of test analysis and technology computer-aided design (TCAD)

†Corresponding author. E-mail: lixuyang@xatu.edu.cn
‡Corresponding author. E-mail: znyu@bit.edu.cn

© 2025 Chinese Physical Society and IOP Publishing Ltd. All rights, including for text and data mining, AI training, and similar technologies, are reserved.

simulation. On the one hand, the HfO_2 modification layer can make the surface of the active layer smoother, improving the carrier transport efficiency. On the other hand, a suitably thick HfO_2 modification layer increases the carrier concentration within the active layer. However, an overly thick modification layer introduces too many acceptor defect states and increases the difficulty of current tunneling between the active layer and the electrode. This work provides a new theoretical basis and experimental approach for the realization of high-performance TFTs. We also fabricated the optimized TFTs into a single-device inverter, demonstrating their potential for application in logic circuits.

2. Experiment details

All TFT devices were fabricated using a bottom-gate and top-contact structure, and the fabrication process is shown in Fig. 1. We used heavily doped n-type thermal oxide silicon as the substrate, as shown in Fig. 1(a), where polysilicon was used as the gate electrode and silicon dioxide with a thickness of 100 nm was used as the dielectric layer. The cleaned substrate was placed into a vacuum chamber and sputtered using a shadow mask, as shown in Fig. 1(b). A 20 nm thick IGZO film was sputtered as the active layer, with a sputtering power of 50 W and a flow rate of argon and oxygen of 40 sccm:5 sccm. The base vacuum was set at 5×10^{-4} Pa and the sputtering vacuum was set at 0.8 Pa. The metal element ratio in IGZO target materials is In:Ga:Zn = 1:1:1. After sputtering the IGZO film, the target source was switched, and HfO_2 films with thicknesses of 0 nm, 1 nm, 3 nm, 5 nm and 7 nm were sputtered as the modification layers, with a sputtering power of 45 W and a flow rate of argon and oxygen of 40 sccm:20 sccm. The base vacuum was set at 5×10^{-4} Pa and the sputtering vacuum was set at 0.8 Pa. The sputtered samples were then annealed in a furnace at 300 °C for 1 hour, as shown in Fig. 1(c). After the samples cooled down, we used thermal evaporation to deposit aluminum metal with a thickness of 100 nm as the source electrode and drain electrode. During evaporation, we used a shadow mask to pattern the electrodes, resulting in a channel length of 100 μm and a width of 1000 μm, as shown in Fig. 1(d).

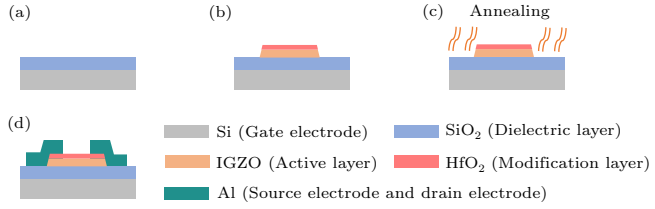


Fig. 1. Fabrication process of IGZO TFTs. (a) Substrate. (b) Sputtering of IGZO film and HfO_2 film. (c) Thermal annealing. (d) Evaporation of source electrode and drain electrode.

The electrical performance of the devices was tested using a Keithley 2636B in a room-temperature dark environment. The surface morphology of the active layer was observed using an atomic force microscope (AFM, Bruker Dimension ICON) to study the quality of the film. The chemical state of the films was analyzed using x-ray photoelectron spectroscopy (XPS, Thermo Scientific K-Alpha). The changes in the carrier concentration within the active layer were analyzed using TCAD simulation.

3. Results and discussion

We first conducted atomic force microscopy (AFM) measurements on the sample surface within a 2 μm × 2 μm scan area, and the results are presented in Figs. 2(a)–2(e). The numerical values labeled in the figures correspond to the HfO_2 film thicknesses, and this labeling convention is maintained throughout subsequent figures. Based on the AFM images of the samples, we were able to calculate the root mean square (RMS) value of the surface roughness of the samples, as shown in Fig. 2(f). As can be clearly seen from Fig. 2(f), the active layer modified with HfO_2 has a lower surface roughness. We propose that during HfO_2 sputtering, the plasma generated in the vacuum chamber may effectively repair the IGZO surface defects. Consequently, compared with unmodified films, the RMS value of the active layer with 1 nm HfO_2 deposition decreases significantly. Moreover, as the thickness of HfO_2 increased, the continuity of the HfO_2 film was enhanced, further smoothing the sample surface. After plasma modification, the smooth interlayer interface helps to reduce the interface trapping effect and promote charge injection and transport,[31,32] which is beneficial to improve the electrical performance of the devices.

We fabricated all samples into TFT devices and evaluated their output characteristics, and the results are shown in Figs. 3(a)–3(e). All samples demonstrated n-type TFT performance with clear pinch-off voltages. At low source–drain voltage (V_{DS}), the source–drain current (I_{DS}) rose linearly with V_{DS}, indicating good ohmic contact between the electrodes and the active layer.[33–35] At high V_{DS}, I_{DS} showed a significant saturation phenomenon. The output characteristic curves of all samples at a gate voltage (V_{GS}) of 40 V are shown in Fig. 3(f), and we extracted the linear part of the curves. We compared the I_{DS} values of the samples when V_{DS} was 10 V. We found that the I_{DS} value of the sample was the highest when the thickness of HfO_2 was 3 nm; when the thicknesses of HfO_2 were 5 nm and 7 nm, the I_{DS} values of the samples decreased significantly.

We further evaluated the transfer characteristics of the devices at a fixed V_{DS} of 10 V, as depicted in Fig. 4. According to the transfer characteristic curves, all the samples exhibited switching characteristics, with a switching ratio greater than 10^5. Notably, at $V_{GS} = 40$ V, the I_{DS} variation trend aligned with that in Fig. 3(f). Based on the transfer characteristic curves, we were able to calculate the electrical parameters

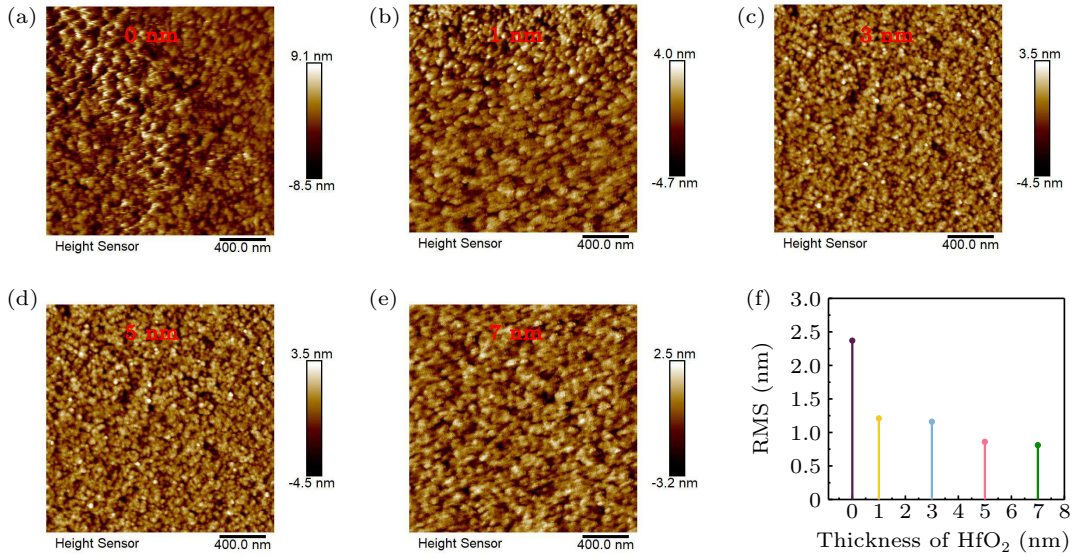


Fig. 2. (a)–(e) AFM images of IGZO with HfO_2 thickness ranging from 0 nm to 7 nm. (f) Root mean square (RMS) surface roughness of the samples.

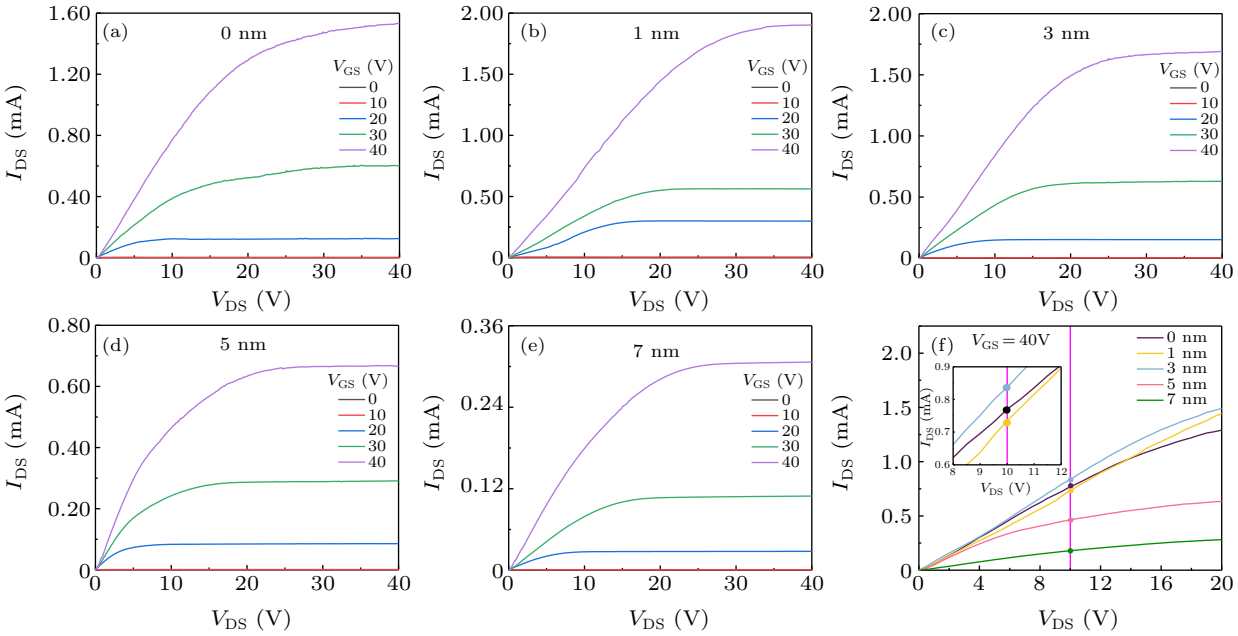


Fig. 3. (a)–(e) Output characteristic curves of IGZO TFTs with HfO_2 thickness ranging from 0 nm to 7 nm. (f) Output characteristic curves at $V_{GS} = 40$ V for all samples.

Table 1. The electrical parameters of TFTs.

Thickness of HfO_2 (nm)	μ_{FE} ($cm^2 \cdot V^{-1} \cdot s^{-1}$)	V_{TH} (V)	SS (V/dec)	I_{on}/I_{off}
0	14.9	0.90	0.63	7.54×10^7
1	17.2	2.33	0.69	6.24×10^7
3	29.6	2.95	0.73	9.23×10^7
5	21.6	5.75	1.09	4.29×10^7
7	12.0	6.68	1.22	9.95×10^5

of the devices such as the field-effect mobility (μ_{FE}), threshold voltage (V_{th}), subthreshold swing (SS) and switching ratio (I_{on}/I_{off}). The electrical parameters of the samples are shown in Table 1.

As shown in Table 1, the mobility of the samples first rose with the increase in HfO_2 thickness. However, when the thickness of HfO_2 exceeded 3 nm, the mobility of the samples decreased with the increase in HfO_2 thickness. We attribute this to HfO_2 altering the oxygen vacancy concentration in the IGZO film, as depicted in Fig. 5. The Hf–O bond strength (802 kJ/mol) far exceeds that of the In–O (346 kJ/mol), Ga–O (374 kJ/mol) and Zn–O (284 kJ/mol) bonds.[36–38] During annealing, some weak metal-oxygen bonds in the IGZO film broke, creating oxygen vacancies, while the released oxygen combined with hafnium to form stable Hf–O bonds. As the thickness of HfO_2 increased, the oxygen vacancy concentration in the IGZO film continuously increased. The increase in oxygen vacancy concentration increases the electron concentration in the channel.[28,39] According to the percolation model, the mobility of amorphous oxide semiconductors will

increase with the increase in carrier concentration.[40,41] This explains why the mobility of the devices increased with the increase in HfO_2 thickness when the thickness of HfO_2 was less than or equal to 3 nm. However, as the oxygen vacancy concentration further increased, more band tail states were introduced in the active layer.[42] These defect states act as scattering centers, increasing carrier scattering during transport and capturing carriers, thus reducing mobility. The subthreshold swing increase with HfO_2 thickness also indicates rising defect state concentration. The difficulty of electron tunneling between the active layer and the electrode also increased with the increase in HfO_2 thickness, and the increase in threshold voltage with the increase in HfO_2 thickness confirmed this point. In other words, the HfO_2 film exhibited increasingly stronger insulating properties as its thickness increased. This also had a negative impact on the mobility of the device. When the thickness of HfO_2 was 7 nm, the threshold voltage had already reached 6.68 V and the switching ratio was only in the order of 10^5.

To verify the above analysis, all samples were tested by x-ray photoelectron spectroscopy (XPS). The O 1s spectra of all samples are shown in Figs. 6(a)–6(e). By deconvoluting the O 1s spectra with a Gaussian function, three sub-peaks with binding energies at 530.3 ± 0.1 eV, 531.9 ± 0.1 eV and 532.8 ± 0.1 eV were obtained. These three sub-peaks correspond to oxygen bonded to metal (M–O–M), oxygen vacancies (M–V_O) and hydroxyl groups (M–OH).[25] The variation trend of the area ratios of the three sub-peaks is shown in Fig. 6(f). When the thickness of HfO_2 was less than or equal to 3 nm, the oxygen vacancy content increased stepwise. This trend was consistent with the previous analysis, indicating that the deposited HfO_2 introduced extra oxygen vacancies into IGZO. However, when the thickness of HfO_2 exceeded 3 nm, the concentration of oxygen vacancies did not increase significantly but rather showed a downward trend, which was

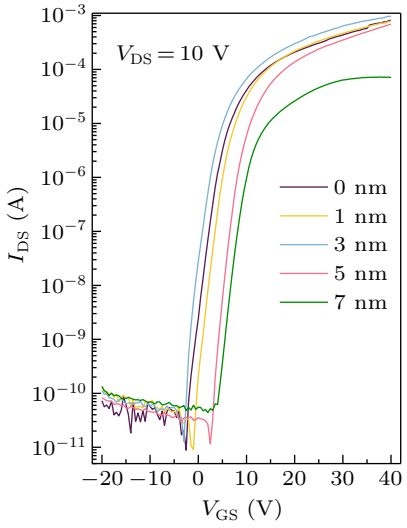


Fig. 4. The transfer characteristic curves for all samples.

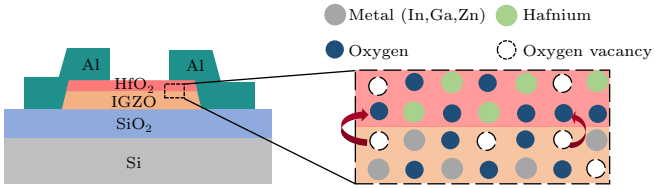


Fig. 5. Schematic cross-section of IGZO TFTs and mechanism of oxygen vacancy formation in the active layer.

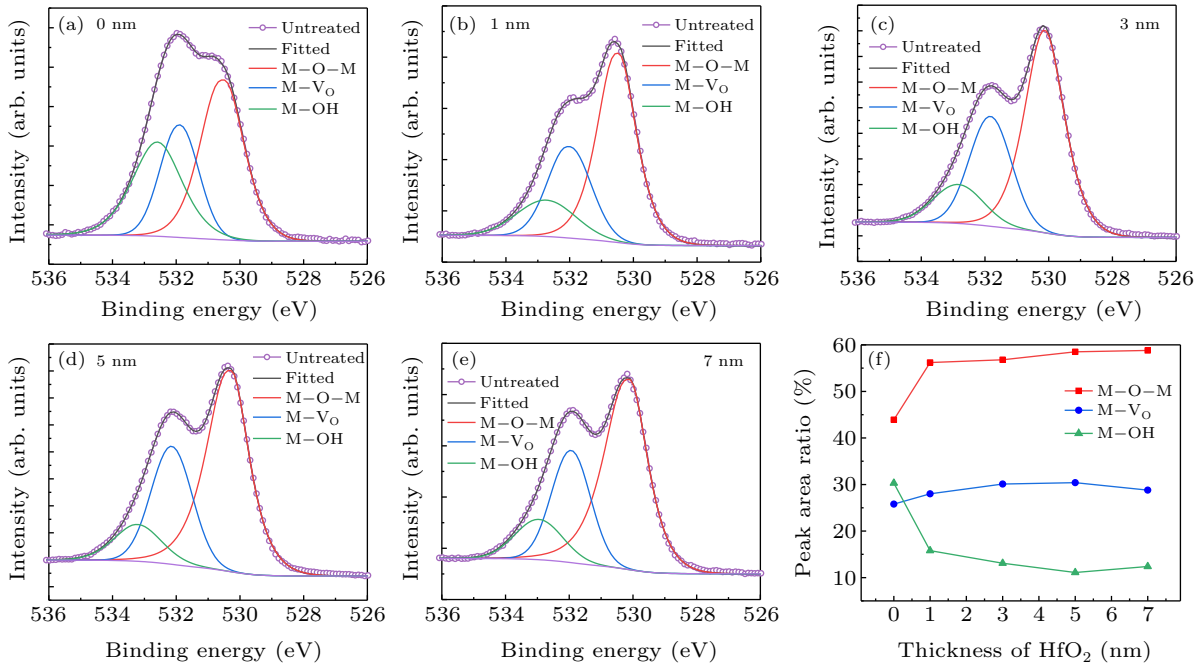


Fig. 6. (a)–(e) O 1s spectra of samples with HfO_2 thickness of 0–7 nm. (f) Trend of sub-peaks for all samples.

inconsistent with the previous analysis trend. This is because XPS tests the surface of the samples. The information collected by the O 1s spectrum is approximately a 10 nm thick film. Since Hf has a higher affinity for oxygen, although the concentration of oxygen vacancies in the IGZO film increases, Hf also combines with oxygen from the air to form metal-oxygen bonds. That is, when the thickness of HfO_2 exceeds 3 nm, although the concentration of oxygen vacancies in the IGZO film increases stepwise, the concentration of oxygen vacancies in HfO_2 is relatively low due to the higher proportion of metal-oxygen bonds in HfO_2. As a result, statistically, the concentration of oxygen vacancies appears to decrease rather than increase. This can be proved by the increasing content of metal-oxygen bonds.

To verify the effect of HfO_2 thickness on the electron concentration in the active layer, we conducted TCAD simulations, as shown in Fig. 7. Figure 7(a) shows the simulated cross-sectional view of the IGZO TFTs. The active layer parameters were set based on Fung *et al.*'s work,[41] including the effective density-of-states (DOS) in the conduction and valence bands, electron affinity, etc. The specific parameters are given in Table 2. Figure 7(b) shows the local enlargement of the active layer and the modifying layer, where the thickness of HfO_2 was set at 0 nm, 1 nm, 3 nm, 5 nm and 7 nm, respectively. Figure 7(c) illustrates the device structure mesh division. The electrode region has a relatively sparse mesh for rougher calculations, while the active and modifying layers have a denser mesh for more detailed calculations. Figure 7(d) shows the electron concentration distribution map in the device after setting V_{GS} at 40 V and V_{DS} at 10 V and running the calculation.

The electron concentration distribution maps allow quantitative analysis of how electron concentration varies with film depth, as depicted in Figs. 8(a)–8(e). By integrating these data, the electron concentration of different samples can be quantitatively determined, as shown in Fig. 8(f). Figure 8(f) reveals that the electron concentration in IGZO peaks at a HfO_2 thickness of 3 nm is consistent with prior analysis. This proves that when the thickness of HfO_2 is less than or equal to 3 nm, HfO_2 will enhance the carrier concentration in the active layer, thereby increasing the mobility of the device. However, when the thickness of HfO_2 exceeds 3 nm, not only will the additional oxygen vacancies capture carriers, leading to a decrease in electron concentration, but the overly thick HfO_2 film also reduces the injection efficiency of source charge due to its strong insulating properties.

Table 2. Partial simulation parameters of the device.[41]

Symbol	Value	Unit	Description
N_c	5×10^{18}	cm^{-3}	effective conduction band DOS
N_v	5×10^{18}	cm^{-3}	effective valence band DOS
g_{ta}	1.55×10^{20}	$cm^{-3}\cdot eV^{-1}$	density of tail states at $E=E_c$
g_{td}	1.55×10^{20}	$cm^{-3}\cdot eV^{-1}$	density of tail states at $E=E_v$
E_a	13	meV	conduction-band-tail slope
E_d	120	meV	valence-band-tail slope
E_g	3.05	eV	band gap
χ	4.16	eV	electronic affinity
ε	1		permittivity
μ_n	15	$cm^2\cdot V^{-1}\cdot s^{-1}$	band mobility (electron)
μ_p	0.1	$cm^2\cdot V^{-1}\cdot s^{-1}$	band mobility (hole)
m_c	0.34	m_e	conduction band effective mass

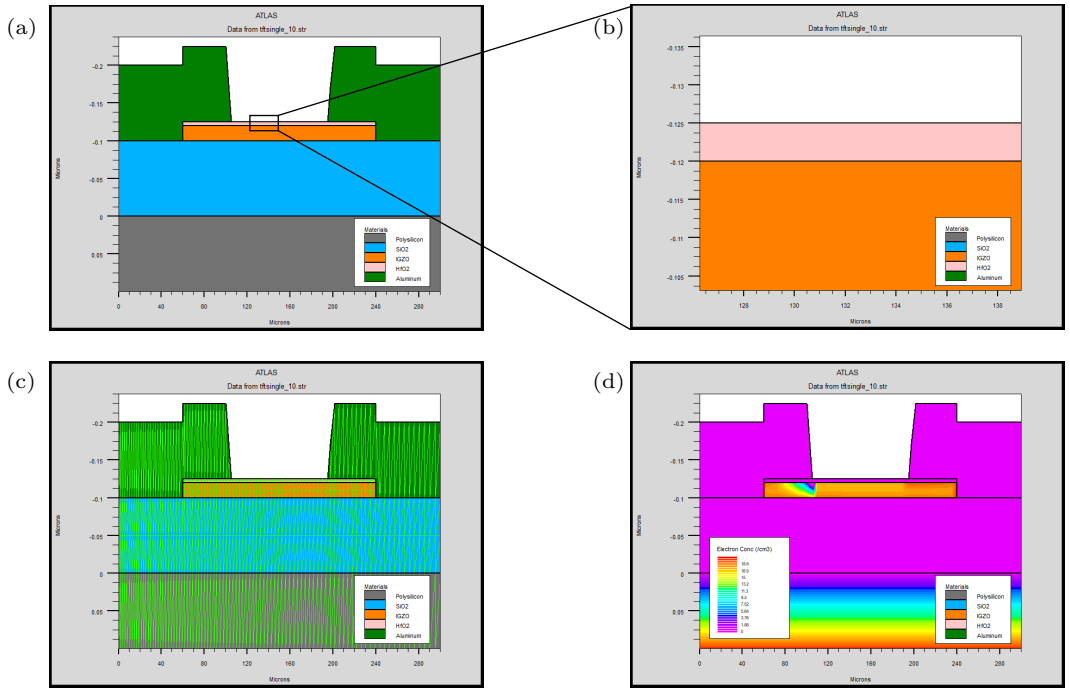


Fig. 7. (a) Simulated structure of IGZO TFT and (b) local magnified image. (c) Grid division. (d) Electronic concentration distribution.

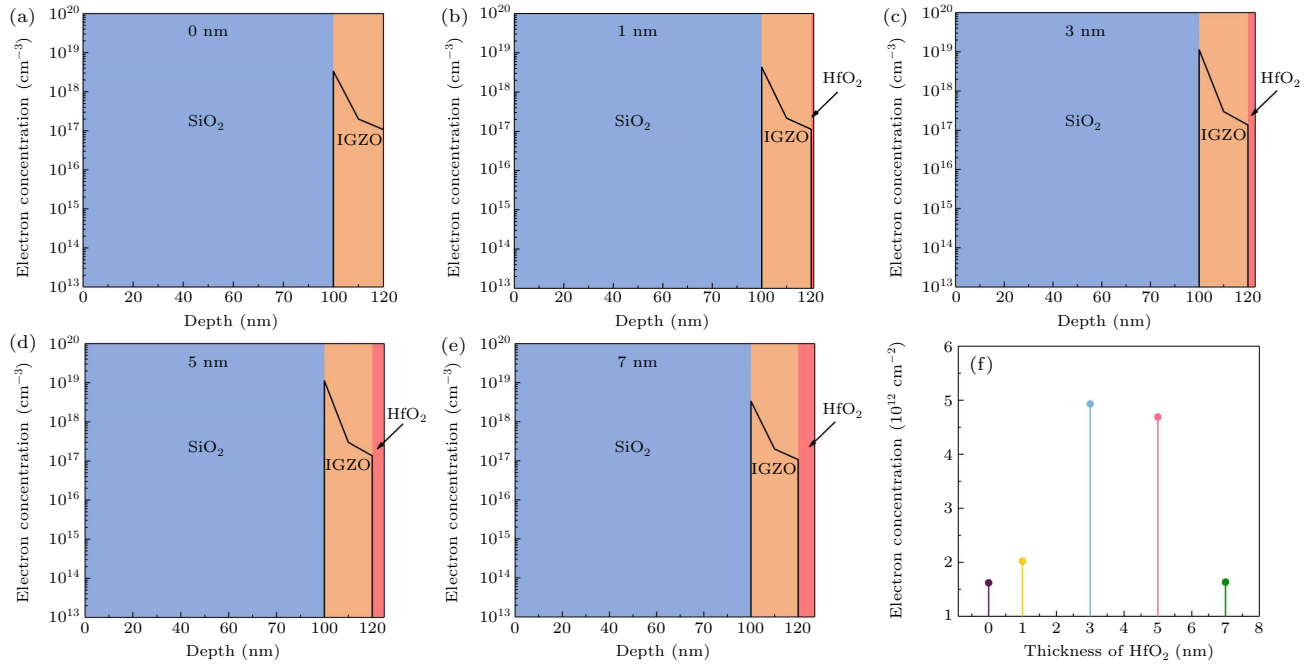


Fig. 8. (a)–(e) The trend of electron concentration changes in all samples. (f) The electron concentration of all samples.

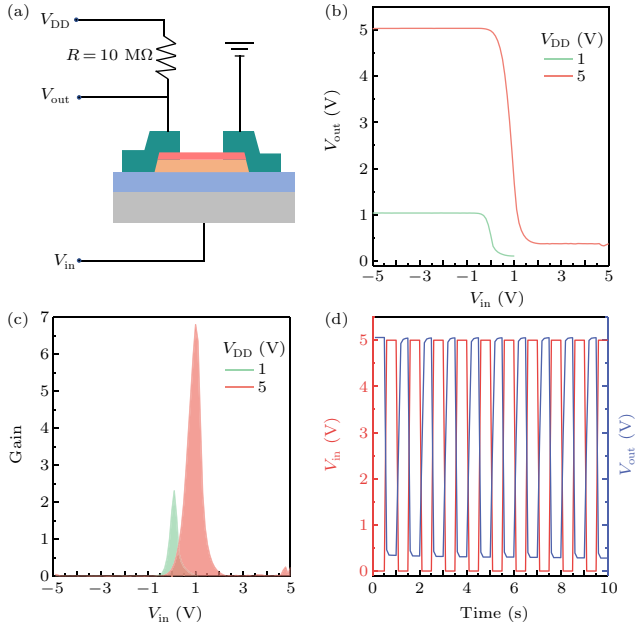


Fig. 9. (a) Single device inverter structure. (b) Voltage input–output characteristic curves. (c) Inverter gain characteristics. (d) Inverter switching characteristics under 1 Hz square wave.

In summary, when the thickness of HfO_2 is 3 nm, the overall performance of the device is optimal. We fabricated a single-device inverter using the sample with a modifying layer thickness of 3 nm to test its feasibility for application in logic circuits.

As shown in Fig. 9(a), we fabricated an inverter using the IGZO TFT with an HfO_2 thickness of 3 nm. V_{in} is the input voltage terminal, V_{out} is the output voltage terminal and V_{DD} is the operating voltage. We tested its voltage transfer characteristics by setting V_{DD} at 1 V and 5 V, respectively, and the results are shown in Fig. 9(b). When V_{in} is 0 V, V_{out} is approximately equal to V_{DD}, and V_{out} is at a high logic level; when V_{in} is equal to V_{DD}, V_{out} is approximately equal to 0 V, and V_{out} is at a low logic level. Thus, the device meets the inverter's logic output requirements. The gain can be obtained by differentiating the voltage transfer characteristic curve. As shown in Fig. 9(c), the gain of the device is much greater than 1, indicating its potential to drive complex logic circuits.[43] We also assessed the inverter's dynamic response, as shown in Fig. 9(d), and it exhibited a good dynamic response under a 1 Hz AC square wave. In summary, the HfO_2-optimized IGZO TFT has great potential for application in logic circuits.

4. Conclusion

In this paper, we introduced a method to modify the active layer of IGZO TFTs using ultra-thin HfO_2 films. We found that the comprehensive performance of IGZO TFTs was optimal when the thickness of the HfO_2 film was 3 nm. Compared with the unmodified control samples, the mobility of the TFTs modified by the HfO_2 film was doubled (14.9 $cm^2 \cdot V^{-1} \cdot s^{-1} \rightarrow$ 29.6 $cm^2 \cdot V^{-1} \cdot s^{-1}$). This improvement can be attributed to two factors. First, the dense oxide film can heal the active layer's surface morphology, reducing roughness and enhancing carrier transport efficiency. Second, the strong Hf–O bonds can introduce more oxygen vacancies into the active layer. An appropriate concentration of oxygen vacancies increases the carrier concentration within the active layer, thereby enhancing device mobility. In addition, we fabricated the optimized device into a single-device inverter, which exhibited good performance and demonstrated the application potential of TFTs in logic circuits. This paper provides a new exper-

imental idea and theoretical foundation for the fabrication of high-performance TFTs.

Acknowledgments

Project supported by the National Natural Science Foundation of China (Grant No. 62441407), the Natural Science Basic Research Program of Shaanxi (Grant No. 2024JC-YBQN-0631), the Natural Science Foundation of Shaanxi Provincial Department of Education (Grant No. 23JK0482), and the Shaanxi Province Key R & D Program General Project - Industrial Field (Grant No. 2024GX-YBXM-085).

References

[1] Saha J K, Billah M M and Jang J 2021 *ACS Appl. Mater. Interfaces* **13** 37350
[2] Zhang S, Weng L, Liu B, Kuang D, Liu X W, Jiang B Q, Zhang G C, Bao Z C, Yuan G C, Guo J, Ning C, Shi D W and Yu Z N 2023 *Vacuum* **215** 112225
[3] Seul H J, Kim M J, Yang H J, Cho M H, Song W B and Jeong J K 2020 *ACS Appl. Mater. Interfaces* **12** 33887
[4] Nomura K, Ohta H, Takagi A, Kamiya T, Hirano M and Hosono H 2004 *Nature* **432** 488
[5] Xu X, He G, Wang L, Wang W, Jiang S and Fang Z 2023 *J. Mater. Sci. Technol.* **141** 100
[6] Park J, Go S, Chae W, Ryoo C I, Kim C, Noh H, Kim S, Du A B, Cho I T, Yun P S, Bae J U, Park Y S, Kim S and Kim D H 2024 *Sci. Rep.* **14** 10067
[7] Xiong W, Huo J Y, Wu X H, Liu W J, Zhang D W and Ding S J 2023 *Chin. Phys. B* **32** 018503
[8] Song S, Liang H L, Huo W X, Zhang G, Zhang Y H, Wang J W and Mei Z X 2024 *Chin. Phys. Lett.* **41** 068501
[9] Yang G, Song W, Yu Z, Huang T, Cao J, Xu Y, Sun H, Sun W and Wu W 2024 *IEEE Trans. Electron Devices* **71** 2990
[10] Weng L, Zhang S, Kuang D, Liu B, Liu X W, Jiang B Q, Zhang G C, Bao Z C, Ning C, Shi D W, Guo J, Yuan G C and Yu Z N 2023 *IEEE Trans. Electron Devices* **70** 4186
[11] Um J G, Jeong D Y, Jung Y, Moon J K, Jung Y H, Kim S, Kim S H, Lee J S and Jang J 2018 *Adv. Electron. Mater.* **5** 1800617
[12] Huang W C, Li Y, Chang N H, Hong W J, Wu S Y, Liao S Y, Hsueh W J, Wang C M and Huang C Y 2024 *Sens. Actuators B: Chem.* **417** 136175
[13] Kim M Y, Kim H W, Oh C, Park S H and Kim B S 2023 *ACS Appl. Mater. Interfaces* **6** 435
[14] Lee S H, Lee S, Jang S C, On N, Kim H S and Jeong J K 2021 *J. Alloys Compd.* **862** 158009
[15] Kwon J Y and Jeong J K 2015 *Semicond. Sci. Technol.* **30** 024002
[16] He F, Wang Y, Yuan H, Lin Z, Su J, Zhang J, Chang J and Hao Y 2021 *Ceram. Int.* **47** 35029
[17] Han Z, Han J and Abliz A 2024 *Appl. Surf. Sci.* **648** 158995
[18] Wu J L, Lin H Y, Su B Y, Chen Y C, Chu S Y, Liu S Y, Chang C C and Wu C J 2014 *J. Alloys Compd.* **592** 35
[19] Lee H, Lee S, Kim Y, Siddik A B, Billah M M, Lee J and Jang J 2020 *IEEE Electron Device Lett.* **41** 1520
[20] Park J C and Lee H N 2012 *IEEE Electron Device Lett.* **33** 818
[21] Bae S D, Kwon S H, Jeong H S and Kwon H I 2017 *Semicond. Sci. Technol.* **32** 075006
[22] Shan F, Lee J Y, Kim H S, Sun H Z, Choi S G, Heo K J, Koh J H and Kim S J 2021 *Electron. Mater. Lett.* **17** 222
[23] Cheng J, Yu Z, Li X, Guo J, Yan W, Xue J and Xue W 2018 *IEEE Trans. Electron Devices* **65** 136
[24] Hu M, Xu L, Zhang X, Song Z and Luo S 2022 *Appl. Surf. Sci.* **604** 154621
[25] Kim J W and Lee S Y 2024 *J. Korean Ceram. Soc.* **61** 941
[26] Nguyen A H T, Nguyen M C, Nguyen A D, Park N H, Jeon S J, Kwon D and Choi R 2023 *IEEE Trans. Electron Devices* **70** 1085
[27] Zhou X, Han D, Dong J, Li H, Yi Z, Zhang X and Wang Y 2020 *IEEE Electron Device Lett.* **41** 569
[28] Park J M, Kim H D, Jang S C, Kim M J, Chung K B, Kim Y J and Kim H S 2020 *IEEE Trans. Electron Devices* **67** 4924
[29] Zhang S, Liu B, Zhang X, Wen C Y, Sun H R, Liu X W, Yao Q, Zi X R, Bao Z C, Xiao Z R, Zhang Y S, Yuan G C, Guo J, Ning C, Shi D W, Wang F and Yu Z N 2024 *Mater. Sci. Semicond. Process* **173** 108093
[30] Kim J, Park J B, Zheng D, Kim J S, Cheng Y, Park S K, Huang W, Marks T J and Facchetti A 2022 *Adv. Mater.* **34** 2205871
[31] Zhang Q, Xia G, Li H, Sun Q, Gong H and Wang S 2024 *Nanotechnology* **35** 125202
[32] Liu A, Liu G, Zhu H, Shin B, Fortunato E, Martins R and Shan F 2016 *J. Mater. Chem. C* **4** 4478
[33] Kai Y, Zhao Y, Wang J, Lu C, Shan Y, Guo Z, Jiang C and Li L 2022 *IEEE Electron Device Lett.* **43** 1681
[34] Chen Y, Duan X, Ma X, Yuan P, Jiao Z, Shen Y, Chai L, Luan Q, Xiang J, Geng D, Wang G and Zhao C 2024 *J. Semicond.* **45** 072301
[35] Xiao N, Yuvaraja S, Chettri D, Liu Z, Lu Y, Liao C, Tang X and Li X 2023 *J. Phys. D: Appl. Phys.* **56** 425102
[36] Xiao B, Yu X and Watanabe S 2019 *ACS Appl. Electron. Mater.* **1** 585
[37] You B C, Wang S J, Ko R M, Wu J H and Lin C E 2020 *Jpn. J. Appl. Phys.* **59** SGGJ03
[38] Lee K M, Kim N, Lee J K, Lee H J, Kim S Y and Kim T G 2025 *Appl. Surf. Sci.* **686** 162102
[39] Socratous J, Banger K K, Vaynzof Y, Sadhanala A, Brown A D, Sepe A, Steiner U and Sirringhaus H 2015 *Adv. Funct. Mater.* **25** 1873
[40] Nomura K, Kamiya T, Ohta H, Ueda K, Hirano M and Hosono H 2004 *Appl. Phys. Lett.* **85** 1993
[41] Kamiya T, Nomura K and Hosono H 2009 *J. Disp. Technol.* **5** 462
[42] Kim D G, Lee W B, Lee S, Koh J, Kuh B and Park J S 2023 *ACS Appl. Mater. Interfaces* **15** 36550
[43] Zhang T, Wei Y F, Zhang C S, He G, Li T J and Lin D 2024 *ACS Appl. Mater. Interfaces* **16** 36577